Accepted version:
Published in : " I*norganic Chemistry* **2020,** *59* (14), 10048-10058"
https://doi.org/10.1021/acs.inorgchem.0c01197

Redox chemistry and reversible structural changes in rhombohedral VO_2F high-energy density cathode during Li intercalation probed by neutron diffraction, *in operando* high-resolution synchrotron X-ray diffraction and soft X-ray absorption spectroscopy

Alois Kuhn,[†*] Michael R. Plews,[‡] Juan Carlos Pérez-Flores,[†#] François Fauth,[⊥] Markus Hoelzel,[§] Jordi Cabana[‡] and Flaviano García-Alvarado[†]

[†] Universidad CEU San Pablo, Facultad de Farmacia, Departamento de Química y Bioquímica, 28668 Boadilla del Monte, Madrid, Spain. E-mail: akuhn@ceu.es

[‡] University of Illinois at Chicago, Department of Chemistry, Chicago IL 60607, USA. E-mail: jcabana@uic.edu

[⊥] Experiments Division, CELLS - ALBA synchrotron, E-08290 Cerdanyola del Vallès, Barcelona, Spain

[§] Forschungsneutronenquelle Heinz-Maier-Leibniz (FRM II), Technische Universität München, D-85747 Garching, Germany

* corresponding author

Present address Juan Carlos: Univ. Castilla-La Mancha, Renewable Energies Inst., Energy Materials Department, 02007, Albacete, Spain

Accepted version:
Published in : " I*norganic Chemistry* **2020,** *59* (14), 10048-10058"
https://doi.org/10.1021/acs.inorgchem.0c01197

Electronic supplementary information (ESI) available. See DOI:

ABSTRACT

Metal oxyfluorides are currently attracting much attention for next-generation rechargeable batteries because of their high theoretical capacity and resulting high energy density. Rhombohedral VO_2F is promising because it allows two electron transfer during electrochemical lithium cycling, with a theoretical capacity of 526 mAh g^{-1}. However, the chemical changes it undergoes during operation are not clearly understood. In this work, a combination of synchrotron X-ray and neutron diffraction was employed to accurately describe the crystal structure of both pristine and lithiated VO_2F, using samples with high crystallinity to overcome challenges in previous studies. The mechanism and reversibility of the lithium insertion was monitored in real time by high angular synchrotron diffraction measurements, performed operando on a lithium battery in the high voltage range, 3.9-2.3 V. Insertion of up to one lithium ion proceeds through a solid-solution reaction, while Rietveld refinements of neutron powder diffraction data revealed that the lithiated states adopt the non-centrosymmetric R3c framework, uncovering an octahedral Li-$(O/F)_6$ coordination with reasonable Li-O/F bond lengths. This work further evaluates the redox changes of VO_2F upon Li intercalation. By comparing changes in electronic states of all the elements in the compound, it clarifies the critical role of both anions, O and F, in the charge compensation, through their covalent interactions with the 3d states of V. The clear evidence of participation of F challenges existing assumptions that its high electronegativity renders this anion largely a spectator in the redox reaction.

Keywords: vanadium dioxyfluoride, transition metal oxyfluorides, lithium intercalation, *in operando* SXRD, neutron powder diffraction, metal-ligand hybridization, XAS

Accepted version:
Published in : " I*norganic Chemistry* **2020,** *59* (14), 10048-10058"
https://doi.org/10.1021/acs.inorgchem.0c01197

Introduction

Rechargeable lithium-ion batteries (LiB) number among the most successful technologies for electrochemical energy storage.[1] To fulfill the demands of a steadily growing demand for energy storage, the development of new electrode materials for next-generation batteries with high energy, high power, enhanced safety, good thermal and mechanical stability, and improved cyclability are required.[2-4] Transition metal fluorides, with a strong ionicity of the M−F bond, could offer a higher average working potential than oxide compounds. A clear proof that fluorine ligands have an increasing effect on the redox potential is found for instance for octahedrally coordinated $Ti^{IV/III}$-O_6 in $Li_4Ti_5O_{12}$ spinel and $Li_2Ti_3O_7$ ramsdellite oxides,[5,6] which increases by notable 1.3 V for $Ti^{IV/III}$-F_6 in Li_2TiF_6 fluoride.[7]

For some common redox centers operative in high-voltage oxide-based electrodes, namely Mn^{IV}-O_6, Co^{IV}-O_6 and Ni^{III}-O_6, fluoride ligands likely would raise working potential above the stability electrochemical window of the present state-of-the-art organic liquid electrolytes (~ 4.8 V vs. Li^+/Li). Therefore, fluorides of other metals with lower working potential in oxides, vanadium for instance, are worth being investigated as prospective high voltage electrode materials. In this connection, we reported on the electrochemical properties of the fluoride Li_3VF_6 for which V(III) is reversibly reduced to V(II).[8] Reduction occurs in the wide potential range 3.0-1.5 V. Mixed anion chemistry, among which oxyfluorides are attracting much attention for next-generation rechargeable batteries,[9] provides an opportunity to tailor output potential of electrode materials and to investigate the role of the different ligands in the redox chemistry of intercalation materials. An interesting oxyfluoride exhibiting high specific capacity is rhombohedral VO_2F (space group R-3c) synthesized for the first time in our group using a high-

Accepted version:
Published in : " Inorganic Chemistry **2020,** *59* (14), 10048-10058"
https://doi.org/10.1021/acs.inorgchem.0c01197

temperature high-pressure solid-state reaction.[10] Later, VO_2F was also prepared by high-energy ball milling.[11,12] VO_2F was found to cycle about one Li with a sloping voltage profile in the voltage range 3.9 - 2.2 V vs. Li^+/Li, delivering a reversible capacity of about 210 mAh g^{-1} over 15 cycles.[10] XRD studies carried out *ex situ* on cycled electrodes suggested the existence of a continuous solid-solution Li_xVO_2F, with only little changes of lattice parameters. However, when VO_2F prepared by ball-milling was cycled in a the 4.0 – 2.1 V vs. Li^+/Li range, more significant changes in lattice parameters of the rhombohedral framework were observed .[11]

Insertion of 1 Li^+/f.u. (263 mAh g^{-1}) in VO_2F in the 3.9 - 2.2 V vs. Li^+/Li voltage range correlates with the reduction of V^{5+} to V^{4+} as deduced from EELS analysis.[10] When compared with reduction of V^{5+} to V^{4+} in V_2O_5 upon insertion of the same 1 Li^+/f.u. in the 3.6-2.5 V vs. Li^+/Li range, the difference of redox potential is not so significant as one might expect for an oxyfluoride despite the high percentage of fluorine present in vanadium dioxyfluoride. Therefore, it could be hypothesized that the F^- ligand in the case of VO_2F does not participate in the redox chemistry or at least its effect is not evident. This somewhat unexpected observation motivated the present work.

Deep discharge of VO_2F to 1 V provides a higher gravimetric capacity of ~ 460 mAh g^{-1} (~1.75 Li^+/f.u.), which significantly exceeds that of the conventional $LiCoO_2$ and $LiFePO_4$ cathode materials and is comparable with the theoretical capacity of Li_2VO_2F with a disordered cubic rock-salt structure, 462 mAh g^{-1}.[13] The R-3c structure of VO_2F was reported to undergo, upon this extended lithiation, an irreversible structural transformation into an electrochemically active disordered Fm-3m rock-salt phase Li_2VO_2F. More recently, the severe capacity fading observed in Li_2VO_2F upon cycling could be suppressed by modification of the electrolyte concentration.[14] Finally, Wang et al. have investigated the structural stability of VO_2F upon heating and Li cycling.[15]

Accepted version:
Published in : " I*norganic Chemistry* **2020,** *59* (14), 10048-10058"
https://doi.org/10.1021/acs.inorgchem.0c01197

However, the structural and chemical changes VO_2F undergoes during operation are not clearly understood. Significant structural details may have been overlooked owing to low crystallinity of samples prepared by the high-energy ball milling procedure. Furthermore, structural characterization of lithiated materials in previous studies was made using ex situ XRD carried out on cycled electrodes, and different results regarding variation of lattice parameters during lithium insertion of 1 Li^+ per f.u. VO_2F were reported. Particularly, the structural details of the specific crystallographic positions that lithium occupies in intercalated VO_2F have not been revealed yet. Therefore, chemical and structural properties of VO_2F should be precisely re-examined using well-characterized samples.

For all these reasons, we decided to undertake in this work a detailed study of structural changes during Li intercalation of 1 Li^+/f.u. within the R-3c rhombohedral phase. First, we prepared polycrystalline lithium intercalated VO_2F samples by chemical lithiation using highly crystalline materials prepared at high temperature and pressure. We determined the precise crystal structure of Li intercalated VO_2F. The complementary use of SXRD and NPD was especially effective in Li_xVO_2F compounds, because neutrons have little sensitivity to vanadium (contrary to X-rays), whereas X-rays have low sensitivity to lithium (contrary to neutrons). We clarified the intercalation mechanism of VO_2F following structural evolution using *in operando* synchrotron radiation diffraction. Lastly, both pristine and intercalated samples were also analyzed by X-ray absorption spectroscopy (XAS) to observe the changes in covalency in the metal-ligand bonds at different formal oxidation states.[16-18]

Experimental

Accepted version:
Published in : " I*norganic Chemistry* **2020,** *59* (14), 10048-10058"
https://doi.org/10.1021/acs.inorgchem.0c01197

The synthesis of rhombohedral VO_2F was adopted from our previous work, following a procedure at both high temperature and pressure.[10] Combination of XRD, microanalysis and electrochemical tests in lithium batteries have shown that the pristine VO_2F material used in this study is identical to the material we previously reported, including a similarly small amount of high-pressure V_2O_5 [19] as secondary phase in some batches of product. To enhance its electrochemical properties, the as-synthesized material was activated by ball milling VO_2F as described in our previous work.[10]

To preserve a high crystallinity suitable for neutron powder diffraction, lithium intercalated samples were prepared by chemical lithiation of as-made VO_2F with freshly prepared lithium iodide solution (0.1 M in acetonitrile). The VO_2F powder (3 g) was first suspended with a small amount of anhydrous acetonitrile, and lithium iodide solution was slowly added while stirring the mixture. Two Li_xVO_2F samples with nominal compositions x = 0.5 and 1.0 were prepared using the corresponding stoichiometric amounts of lithium iodide. After the reaction mixtures were stirred for 2 weeks at room temperature, samples were filtered, washed repeatedly with acetonitrile and finally dried under vacuum. All sample preparations were carried out in an argon-filled glovebox to prevent reaction of the lithiated compounds with air and moisture. The chemical lithiation is accompanied by a color change of the oxyfluoride from reddish-brown to green-ochre. Lithium contents of the two lithiated samples were checked by Atomic Emission Spectroscopy (AES) and seen to agree with nominal compositions.

High angular resolution neutron powder diffraction (NPD) was performed at SPODI (Heinz Maier-Leibnitz source FRM II, Garching, Germany).[20] Sample compositions x = 0.5 and 1.0 were measured at 300 K in the angular range 3-150º using the wavelength 1.5483 Å selected with a Ge(551) monochromator. Samples were loaded in argon atmosphere in airtight vanadium cans sealed with indium O-rings to prevent them from

Accepted version:
Published in : " I*norganic Chemistry* **2020,** *59* (14), 10048-10058"
https://doi.org/10.1021/acs.inorgchem.0c01197

reaction with moisture and air. Rietveld refinement[21,22] was performed using the Fullprof program.[23] The negative neutron scattering length factor of Li increases considerably the contrast with respect to O atoms, enabling Fourier density map investigations addressed to localize Li atoms. Fourier density difference maps were built using the GFourier package incorporated in Fullprof.[23] The coherent neutron scattering lengths used were: V: −0.3824 fm, Li: −1.90 fm, O: +5.803 fm and F: +5.654.[24] Structural models were visualized using the Vesta software.[25]

Positive electrodes were prepared by mixing VO_2F with conductive carbon black (C-NERGY Super C65, Timcal) and Kynarflex binder in a 75:20:5 weight ratio and pressing the mixture into 8 mm diameter pellets, followed by drying overnight at 80ºC.

The active part of the cell was composed of positive electrode, glass fiber separator (Whatman) soaked with 1 M $LiPF_6$ in ethylene carbonate (EC) and dimethyl carbonate (DMC) (1:1 vol %) as electrolyte and Li metal as negative electrode, assembled in CR2032-type coin cells. For *in situ* measurements, the active stack is inserted between two circular thin pieces of aluminum foil (50 μm), which were used as current collector in both electrodes because of their high transparence to high intensity synchrotron X-rays of high enough energy. Here, circular centered holes (3 mm and 5 mm, respectively) were introduced in both the negative and positive casings and the stainless-steel spacer disk of the coin cell before the assembly of the electrochemical cell inside an Ar-filled glove box. Further details regarding coin cell construction and beamline setup can be found in ref [26,27]. The electrochemical galvanostatic experiment was controlled with a MPG-2 multichannel galvanostat-potentiostat. The VO_2F//Li cell was discharged and charged in the 3.7-2.3 V vs. Li^+/Li voltage range with a current density of 7.5 mA g^{-1} (corresponding to a C/35 rate). This configuration ensured that synchrotron X-ray data of a complete discharge-charge cycle were collected (Figure S1† in the ESI). Compared to VO_2F//Li

Accepted version:
Published in : " I*norganic Chemistry* **2020,** *59* (14), 10048-10058"
https://doi.org/10.1021/acs.inorgchem.0c01197

cells discharged in conventional *ex situ* coin cells, no significant changes of voltage, shape of discharge-charge curves or capacities were observed, indicating that the data collected under this *operando* regime represents the electrochemical behavior of VO_2F electrodes in conventional lithium half cells.

In Operando synchrotron radiation diffraction experiments were performed at the BL04 MSPD beamline of the ALBA synchrotron light facility (Cerdanyola del Vallès, Spain). Transmissions geometry was chosen, going the beam through all the layers of the in-situ cell. The wavelength was λ=0.8253(1) Å throughout the whole experiment, selected by means of a double-crystal Si(111) monochromator. Synchrotron X-ray diffraction patterns were collected in the 2-52º 2θ angular range (d-range: 23.6-0.94 Å) using a 1-D position sensitive detector MYTHEN. This setup allows fast data acquisition with extremely high statistics and good angular resolution.

The full width at half-maximum (fwhm) for representative peaks of pristine VO_2F measured with the in situ cell is 0.047° at 2θ = 12.87°, compared to 0.042º at the same angle for the VO_2F phase measured inside a capillary (this value increases to 0.084º at the highest diffraction angles), and the signal-to-noise ratio for the most intense peak amounts to ~15. The experimental discharge time-to-data acquisition time ratio for a full discharge was ~700. These conditions ensured that highly reliable data with negligible Δx for each diffraction pattern were collected throughout all electrochemical measurements. The quality of the data collected in these conditions allows Rietveld structural refinements of the Li_xVO_2F compounds. As the beam is going through all layers in the battery, additional Bragg reflections from lithium and aluminum (two windows between which the active cell is placed) are generated. The 2θ regions where these peaks occur can be eliminated by comparing the whole pattern obtained in the *in operando* cell with the pure pristine phase. Figure S2† (Supplementary Information) shows the full

Accepted version:
Published in : " Inorganic Chemistry **2020,** *59* (14), 10048-10058"
https://doi.org/10.1021/acs.inorgchem.0c01197

measured 2θ range, in which the positions of the extra Bragg reflections are marked. The absorption of the sample is taken into account using the correction factor for flat-plate samples in transmission geometry. For a correct refinement of data, we followed a protocol similar to that given by M. Bianchini et al.[28] At first, zero-shift was determined using the pristine VO_2F with well-known unit cell parameters. Secondly, this zero-shift parameter was used and fixed throughout all subsequent refinements. The results of refinements of pristine VO_2F from data collected in a capillary and those available from previous reports are compared in Table S1† (Supplementary Information) with actual results using the *in operando* cell. All data treatments were performed using the Fullprof program.[23]

For XAS studies, Li_xVO_2F samples with precise intercalated lithium contents were synthetized by discharging two cells under potentiostatic conditions to 3.2 and 2.2 V, respectively, because they are representative of the different voltage regions observed in the electrochemical curves. A third sample was prepared by discharging a cell to 2.2 V followed by charging to 3.9 V. Cells were run under potentiostatic conditions and discharged or charged to a determined voltage and left to equilibrate until the measured current was < 0.1 μA. The cells were then stopped and disassembled in an argon-filled glovebox. Electrolyte was removed by washing the positive electrodes with dry DMC. To avoid any oxidation or contact with moisture or oxygen during XAS experiments, samples were affixed to carbon tape in an argon filled glovebox. The samples were transferred to beamline 4-ID-C at the Advanced Photon Source, Argonne National Laboratory, in a sealed container and transferred into the sample chamber in a glovebag under a positive pressure of argon. The measurements were collected at 1×10^{-9} Torr (1.3332×10^{-7} Pa), simultaneously in both the total electron yield (TEY) and total fluorescence yield (TFY) mode, mode utilizing photocurrent for the TEY and a silicon

Accepted version:
Published in : " I*norganic Chemistry* **2020,** *59* (14), 10048-10058"
https://doi.org/10.1021/acs.inorgchem.0c01197

drift diode detector for the TFY. Whereas the escape length of photoelectrons dictates a sensitivity to the first 5-10 nm into the sample, fluorescent photons are collected from at least an order of magnitude deeper into the electrode, providing an opportunity to compare portions dominated by its surface and its interior, respectively. Data were obtained at a spectral resolution of ~0.1 eV, with a 2 sec dwell time. 3 scans (2 in the case of F K-edge data) were performed on each sample to verify reproducibility and the absence of beam damage. Subsequently, the scans were averaged in order to maximize the signal to noise ratio. The V $L_{2,3}$- and O *K*-edges were scanned consecutively in one measurement spanning from 505 to 550 eV, whereas data at the F *K*-edge was collected between 680 to 710 eV.

Results and discussion

As-prepared rhombohedral VO_2F exhibits a specific capacity of 87 mAh g^{-1} (0.33 Li / f.u.) in the 4.0-2.2 V range with a sloping voltage profile (Figure S1† in the ESI). After ball milling (1.5 h, 15 Hz), the specific capacity is greatly enhanced to attractive 250 mAh g^{-1} (0.9 Li / f.u.) for the first discharge, as shown in Figure 1, in agreement with our previous results.[10] The corresponding differential capacity *vs.* voltage plot shows a broad reductive peak centered at 3.5 V with its oxidative peak centered at 3.65 V and a very broad feature centered at 2.75 V. A comparison of voltage profiles of non-milled and milled materials (Figure S3†) on one hand, and their corresponding derivative curves (Figure 1 and Figure S4†) shows that the only significant effect of the milling process is an increase of specific capacity. The sloping voltage profile along with its broad derivate curve point to a single-phase (solid solution) reaction in this compositional range ($0 \leq x$

Accepted version:
Published in : " Inorganic Chemistry **2020,** *59* (14), 10048-10058"
https://doi.org/10.1021/acs.inorgchem.0c01197

≤ 0.9). Both non-milled and milled VO_2F exhibit excellent capacity retention in the first cycles, as shown in Figure S2† and Figure 1. Other authors ascribed the poor cycle stability of VO_2F to the partial dissolution in the electrolyte solution.[14] The better cycling characteristics observed here can be attributed to the larger crystal size of our VO_2F obtained at high temperature and pressure avoiding partial dissolution of the material, when compared to the significantly smaller particle size of VO_2F prepared by high-energy mechanical milling.[11,12] In addition, other authors have related the occurrence of a high irreversible capacity to the irreversible phase transformation of rhombohedral VO_2F to cubic $Li_{2-x}VO_2F$ upon extended lithiation.[11, 12, 14]

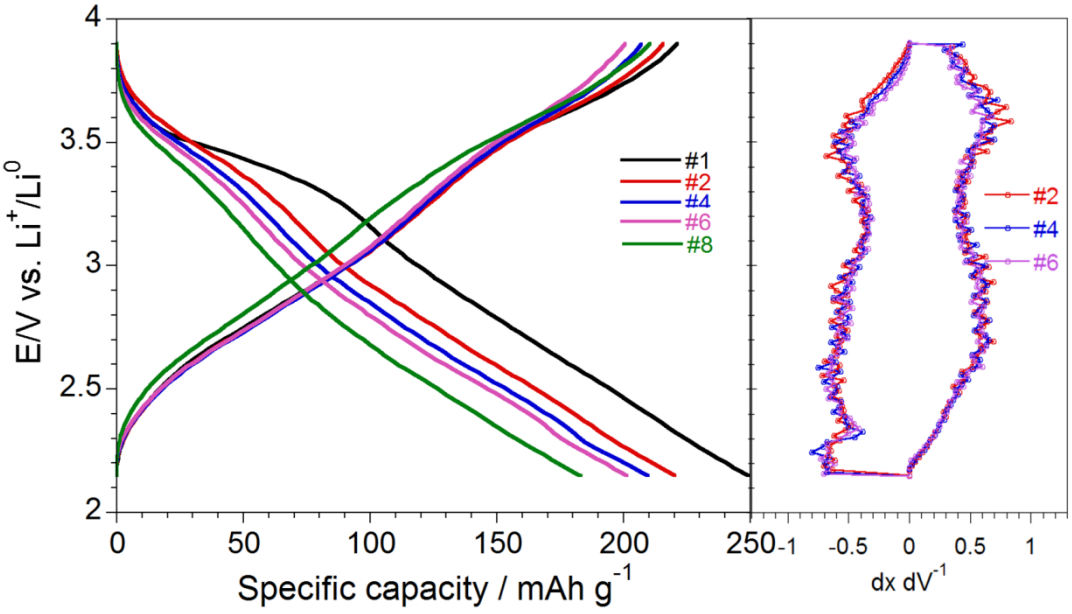

Figure 1: Electrochemical galvanostatic discharge-charge profile of a VO_2F//Li cell at C/20 rate per intercalated Li^+ ion. Selected cycles are shown (left). Inverse derivative curves (dx dV^{-1}) providing details of the electrochemical features are shown for cycles 2,4 and 6 (right).

Neutron diffraction

Accepted version:
Published in : " Inorganic Chemistry **2020,** *59* (14), 10048-10058"
https://doi.org/10.1021/acs.inorgchem.0c01197

The neutron diffraction pattern of pristine VO_2F was completely indexed with space group R-3c, in agreement with our previous work,[10] as shown in Fig. 2. A small amount of β-V_2O_5 as minor secondary phase (~2%) was included in refinements. The refined lattice parameters are $a = b = 5.1310(1)$ Å, $c = 13.0693(2)$ Å, and $V = 297.99(1)$ Å^3, which are consistent with previous reports.[10-12] Vanadium occupies the 6a site (0,0,0) and its atomic displacement parameter was complementarily adapted from a synchrotron X-ray diffraction Rietveld refinement, because its nucleus scarcely scatters neutrons.[24,29] On the other hand, O and F share one anion site at random (18b) with a 2:1 atomic ratio according to nominal composition.

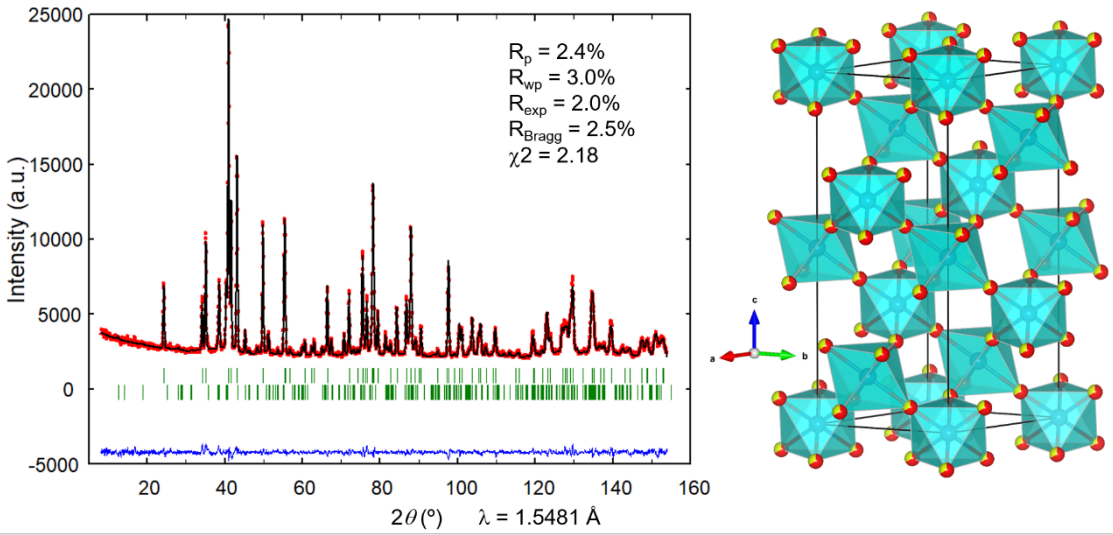

Figure 2: Rietveld-refined fit of the rhombohedral VO_2F structural model (S.G. R-3c) to the neutron diffraction data (left), together with an illustration of the crystal structure for VO_2F (right). The lower Bragg bars correspond to β-V_2O_5 as minor secondary phase.

The crystal structure analysis of two lithium intercalated Li_xVO_2F compounds (x = 0.5 and 1.0), corresponding to intermediate and end compositions of the solid solution, was initiated with the VO_2F framework structure in space group R-3c (Figure 2) using the

Accepted version:
Published in : " I*norganic Chemistry* **2020,** *59* (14), 10048-10058"
https://doi.org/10.1021/acs.inorgchem.0c01197

powder neutron diffraction data collected at 300K. Refined unit cell parameters of pristine VO_2F, $Li_{0.5}VO_2F$ and $LiVO_2F$ are presented in Table 1. It was apparent that the structures of lithiated $Li_{0.5}VO_2F$ and $LiVO_2F$ were closely related to those of VO_2F and many other binary transition metal trifluorides MF_3 (M = Ti, V, Cr, Fe, Co, Ru, Rh, Pd, Ir).[30-33] It is important to note that the Li_xVO_2F compounds reported here only present moderate differences in their lattice parameters. This behavior is similar to that found in our previous work for an electrochemically discharged VO_2F electrode[10]; however, it is different from that reported by Cambaz et al.[11], where a strong change in lattice parameters was found upon electrochemical lithiation. Therefore, we considered very important a deeper understanding of the structural changes that occur during lithiation of VO_2F using *in operando* synchrotron radiation diffraction, results of which will be presented in the next section.

Table 1. Crystallographic data of several Li_xVO_2F compounds obtained from powder ND data at 300K. Previous results from references[10-12] were obtained with powder XRD data. HP: high pressure; BM: ball milling.

Compound	T / K	a (Å)	c (Å)	Volume (Å^3)	c/a
VO_2F, ND (this work)	**300**	**5.1310(1)**	**13.0693(2)**	**297.99(1)**	**2.547**
VO_2F, SXRD (this work)		**5.1322(2)**	**13.0738(5)**	**298.25(2)**	**2.547**
Ref. [10] HP		5.1226(1)	13.0686(3)	296.9(1)	2.551
Ref. [12] BM		5.1374(4)	13.0405(2)	298.06(5)	2.538
Ref. [11], BM		5.12	13.09	296.7	2.56
$Li_{0.5}VO_2F$ this work, ND	**300**	**5.1039(4)**	**13.145(1)**	**296.55(4)**	**2.575**

Accepted version:
Published in : " I*norganic Chemistry* **2020,** *59* (14), 10048-10058"
https://doi.org/10.1021/acs.inorgchem.0c01197

$LiVO_2F$ this work, ND	**300**	**5.1008(6)**	**13.168(2)**	**296.71(7)**	**2.582**
discharge 2.3V, HP [10]		5.1162(9)	13.051(2)	295.9(1)	2.55
discharge 2.5V, BM [12]		5.00	13.68	296.0	2.74
discharge 2.1V, BM [12]		4.98	13.88	298.3	2.78

The lithium site in lithiated VO_2F samples was determined from difference Fourier synthesis maps using the powder ND data. Figure 3 shows the maps of the z = 0.25 section projected onto the xy plane and the x = 0 section projected onto the yz plane, respectively. The negative residual nuclear scattering length density can be clearly observed at the 6a position (0 0 1/4), suggestive of the Li occupation (Figure 3). However, we noticed immediately that Li on this 6a site presents only three reasonable Li-O/F bond lengths (2.015 Å), together with six other very long Li-O/F distances (2.697 Å). Dropping the space group symmetry from R-3c to R3c through elimination of the inversion center creates 6a position at (0 0 ≠1/4). This allows the Li atom (also the anions) to shift away along the z direction from its "ideal" 6a position (0 0 ¼) in space group R-3c, and the lithium position approaches (0 0 ~0.30) in $LiVO_2F$, as illustrated in the difference Fourier map in Figure 3. Lithium can in principle be placed at the same coordinates (0 0 ~0.30) in space group R-3c, which implies splitting of 6a position into 12c positions with 50% occupancy. However, we discarded this possibility because of the resulting very short Li-Li distances (<1.5 Å). It is interesting to note that Li in Li_xVO_2F then occupies the same position as in $LiReO_3$ [34] and $LiNbO_3$.[35]

It must be noted that it is not possible to tell apart space groups R-3c and R3c from powder diffraction data, and other techniques (TEM, single crystal diffraction) should be brought in to resolve this matter. However, the lower symmetry space group R3c allows for a six-fold octahedral coordination for lithium (owing to the extra freedom gained along the z coordinate for lithium and along y and z for the anion site) with reasonable Li-O/F bond

Accepted version:
Published in : " Inorganic Chemistry **2020,** *59* (14), 10048-10058"
https://doi.org/10.1021/acs.inorgchem.0c01197

lengths in the range 2.023-2.216 Å. As a matter of fact, only refinements of lithiated VO_2F compounds performed in the non-centrosymmetric R3c structure satisfy the crystal chemistry requirements for lithium (adequate Li-O/F bond lengths and anion coordination), as shown in Table 3. Interestingly, it is well known that lithium intercalated derivatives of ReO_3 adopt the same space group R3c, in which the undistorted cubic ReO_3 host lattice undergoes significant twisting upon Li insertion, in order to accommodate the coordination preferred by the Li ions.[34,36]

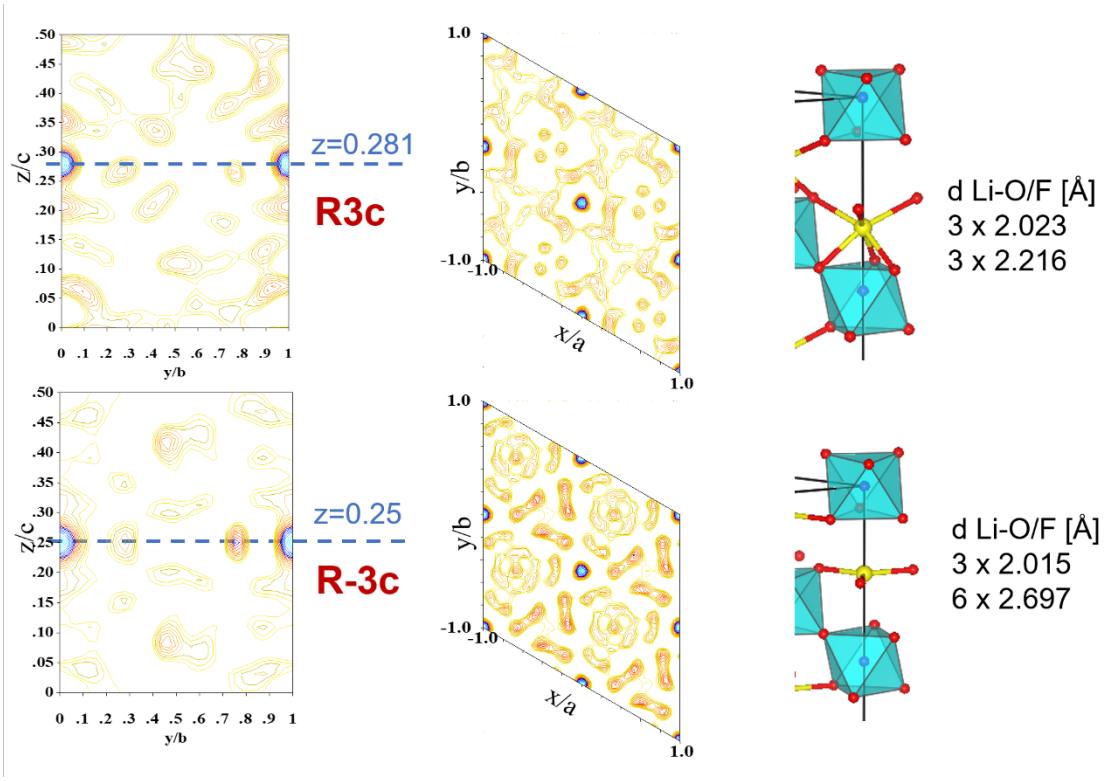

Figure 3: Two-dimensional difference Fourier synthesis maps of $LiVO_2F$ in space group R-3c (bottom) and R3c (top) using the powder ND data of the x = 0 (left) and z = 0.25 (middle) sections, respectively. Derived coordinations for lithium (yellow sphere) with O/F anions (red spheres) are illustrated on the right.

Accepted version:
Published in : " I*norganic Chemistry* **2020,** *59* (14), 10048-10058"
https://doi.org/10.1021/acs.inorgchem.0c01197

Table 2: The structures of VO_2F, $Li_{0.5}VO_2F$ and $LiVO_2F$ using NPD data at 300K. S.G. is R-3c for VO_2F and R3c for Li_xVO_2F.

A. The structure of VO_2F. Space group R-3c (#167)						
Atom	Wyckoff position	Atomic position			B_{iso}	Occ.
		x/a	y/b	z/c		
V	6a	0	0	0	0.8	1.0
O/F	18e	-0.4195(3)	0	0.25	1.0(1)	2/3, 1/3 [1)]
B. The structure of Li_xVO_2F. Space group R3c (#161)						
Atom	Wyckoff position	Atomic position			B_{iso}	Occ.
		x/a	y/b	z/c		
V	6a	0	0	0	0.8	1.0
Li (x=0.5)	6a	0	0	0.333(3)	1.0	0.5
Li (x=1)	6a	0	0	0.290(1)	1.0(1)	1.0
O/F (x=0.5)	18b	-0.4015(3)	0.0104(5)	0.235(1)	1.0(1)	2/3, 1/3 [1)]
O/F (x=1)	18b	-0.3991(3)	0.0039(4)	0.235(1)	1.0(1)	2/3, 1/3 [1)]

1) Anion occupancy fixed according to composition VO_2F

Accepted version:
Published in : " I*norganic Chemistry* **2020,** *59* (14), 10048-10058"
https://doi.org/10.1021/acs.inorgchem.0c01197

Table 3: Bond lengths and angles of VO_2F, $Li_{0.5}VO_2F$ and $LiVO_2F$ as deduced from Rietveld refinement of NPD data at 300 K.

	Lithium coordination polyhedron		
	VO_2F	$Li_{0.5}VO_2F$	$Li_{1.0}VO_2F$
Li-O/F distance [Å]	-	2.12(3) x 3 2.19(1) x 3	2.13(1) x 3 2.17(1) x 3
O/F-Li-O/F angle [º]	-	75.8(1) - 110.3(1)	77.2(1) - 109.5(5)
	Vanadium coordination polyhedron		
V-O/F distance [Å]	1.884(3) x 6	1.827(7) x 3 1.985(9) x 3 Mean: 1.906	1.813(7) 2.012(9) Mean: 1.913
O/F-V-O/F angle [º] V-O/F-V angle [º]	89.9(1) - 90.1(1) 154.7(7)	81.9(1) - 98.0(1) 148.9(6)	83.0(5) - 97.4(5) 147.8(3)
	Metal-metal distance		
Li-V (along *c* axis)	-	3.01(1)	2.76(1)
Li-Li, V-V	3.6770(1)	3.6720(4)	3.6751(4)

Refined atomic positions, cell parameters, and thermal parameters for the Li_xVO_2F structure are presented in Table 2 referred to hexagonal setting of the cell. Reliability factors are summarized together with the graphical results of final refinements in Figure S5†.

The main characteristic of the Li_xVO_2F structure are chains of occupied and vacant face shared V-O/F_6 and Li-O/F_6 octahedra, piled up along the hexagonal *c* axis in the sequence V-Li-vacancy-V-Li-vacancy (Figure 4). Both M-O/F_6 octahedra are irregular, as can be seen in figure 4, which shows the shared triangular faces along the *c* axis, with a more severe distortion of the Li polyhedron, as can be deduced from the O/F-M-O/F angles (Table 3). V-O/F and Li-O/F distances are in the range 1.81 to 2.01 Å and 2.12 to 2.19 Å, respectively. The lengthening of the mean V-O/F from 1.884 Å in pristine VO_2F to 1.913

Accepted version:
Published in : " I*norganic Chemistry* **2020,** *59* (14), 10048-10058"
https://doi.org/10.1021/acs.inorgchem.0c01197

Å in Li_xVO_2F is in agreement with the reduced oxidation state of vanadium upon Li insertion. At the same time, lithiation of VO_2F is related with a distortion of the almost regular V polyhedron found in VO_2F (V-O/F-V angles, Table 3) and a stronger octahedral tilting of the already somehow tilted VO_2F structure, in which the V-O/F-V angles decrease from 154.7º in VO_2F to 147.8º in $Li_{1.0}VO_2F$. The structural refinement from powder neutron diffraction data clearly shows that Li ions in Li_xVO_2F are ordered, and additional Fourier difference maps gave no indication that lithium occupies the empty oxygen octahedra (6a site). Interestingly, these vacant octahedra are occupied by additional lithium in Li_2ReO_3.[34,36] The shift of the anion position is a measure of the degree of octahedral twisting on Li insertion. Specifically, the x coordinate of the general position (x, ~0, ~¼), has a value x = -0.5 in the undistorted cubic ReO_3 structure (3/4 ccp, Pm-3m) and approaches x = -1/3 in the fully twisted rhombohedral RhF_3 structure (hcp, R-3c). As a matter of fact, the octahedral twist in the ReO_3 structure about the cubic (1,1,1) direction transforms the 12-fold coordinated cuboctahedral cavity into two 6-fold coordinated octahedral cavities, appropriate to accommodate Li ions. Pristine VO_2F with x ~ -0.42 already shows some distortion. Li contents up to 1 in Li_xVO_2F reveal a subtle increase of twisting on Li insertion (anion x coordinates are -0.401 in $Li_{0.5}VO_2F$ and -0.399 in $Li_{1.0}VO_2F$). On the other hand, V-V distances (3.677 Å) are not significantly altered during Li uptake.

Accepted version:
Published in : " Inorganic Chemistry **2020,** *59* (14), 10048-10058"
https://doi.org/10.1021/acs.inorgchem.0c01197

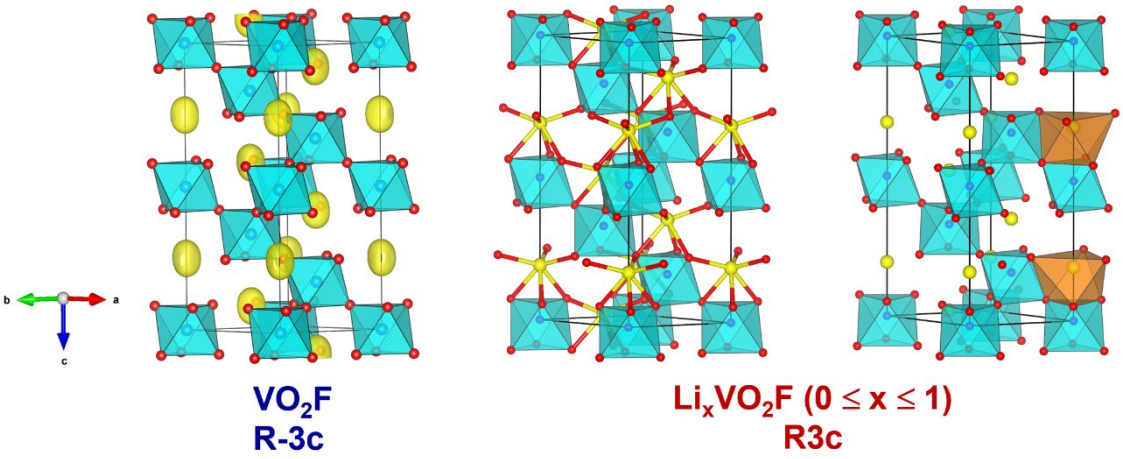

Figure 4: Crystal structures of VO_2F (left) showing the differential bond valence map of lithium (ΔV=0.0 val. units) and lithiated VO_2F (medium and right). V-O/F octahedra (cyan); Li (yellow spheres); O/F (red spheres); Li-O/F octahedra (orange).

It emerges that the lithiated VO_2F compounds of the present work, prepared by a high-temperature high-pressure procedure, show a different structural behavior than the lithiated material studied by Cambaz et al.[11] That author proposed, based on crystal chemistry considerations, the Li to occupy the 6a position (0 0 ¼) in their lithiated VO_2F material after discharging to 2.1 V in a lithium cell. However, only after completing the ¾ ccp into hcp transformation, for example in the completely twisted metal trifluoride RhF_3, would the 6a site be available for lithium with adequate coordination and reasonable bond distances.

To summarize, our neutron diffraction study has demonstrated that VO_2F undergoes little structural changes on chemical Li insertion, in agreement with our previous findings for an electrochemically discharged VO_2F electrode.[10] However, this observation is different from Cambaz et al.[11], where a strong change in lattice parameters was found upon electrochemical lithiation. To further clarify this discrepancy, we monitored the structural

Accepted version:
Published in : " I*norganic Chemistry* **2020,** *59* (14), 10048-10058"
https://doi.org/10.1021/acs.inorgchem.0c01197

changes that occur during lithiation of VO_2F using *in operando* synchrotron X-ray diffraction during a full galvanostatic discharge-charge cycle in the 3.7 - 2.3 V range.

In Operando SXRD study

Figure 5 shows the synchrotron XRD patterns collected upon insertion of lithium until the nominal composition $Li_{0.9}VO_2F$ is reached at the end of the galvanostatic discharge. It is worth pointing out the good quality of the diffraction data in terms of both angular and intensity resolution, indispensable for identifying even very subtle changes occurring in this structure. Table S1† compares refinement results obtained for pristine VO_2F from data collected in capillary with actual results obtained using the *in situ* cell setup. Note that the use of the *in situ* cell only slightly increases the error bars, allowing refinement of atomic parameters. Isotropic thermal factors B_{iso} were refined in initial VO_2F and then fixed to these values for refinements of the following diffraction patterns. No attempts were made to refine lithium atomic parameters.

It strikes immediately that subtle and continuous shifts in diffraction peak positions occur during the first discharge, characteristic of a single-phase (solid solution) mechanism in the $0 \leq x \leq 0.9$ compositional range. The reversible retrogression of Bragg reflections observed upon galvanostatic charge of the cell to diffraction peak positions of pristine VO_2F proves the excellent reversibility of structural changes within this single-phase region. The composition of the material charged to 3.9 V was estimated to be $Li_{0.1}VO_2F$, since a small coulombic inefficiency was observed upon charge (Figure S1†).

Accepted version:
Published in : " Inorganic Chemistry **2020,** *59* (14), 10048-10058"
https://doi.org/10.1021/acs.inorgchem.0c01197

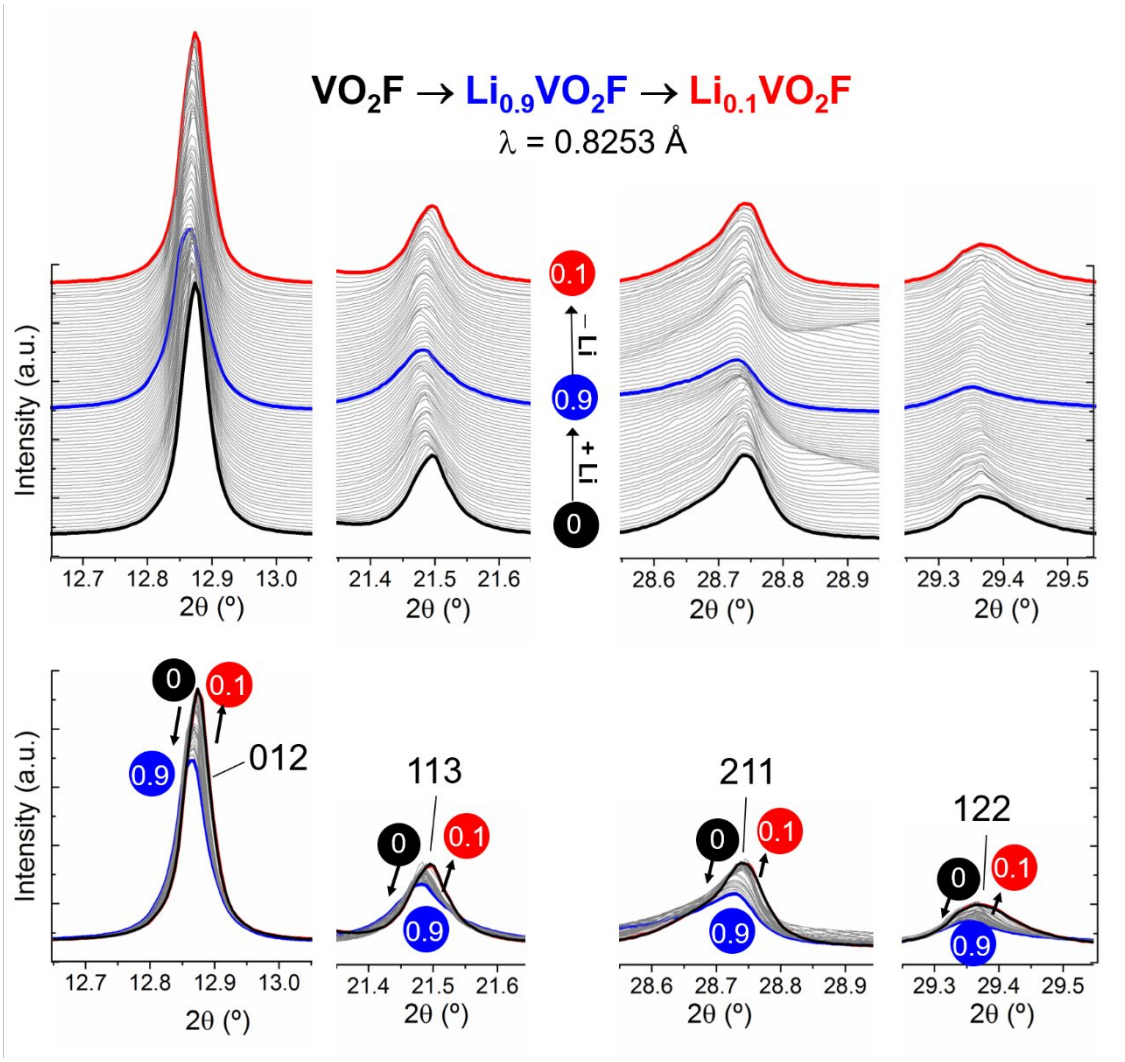

Figure 5: Different angular domains observed during the Li^+ intercalation in rhombohedral VO_2F. The most prominent peaks are indexed. Among all single-phase compositions, the following are highlighted: pristine VO_2F (black, x=0), $Li_{0.9}VO_2F$ (blue) after first discharge and $Li_{0.1}VO_2F$ (red) at the end of first charge.

When the cell voltage is lowered (E < 2.3 V, x > 0.9, Figure S6†), allowing further lithium to be intercalated into VO_2F, it appears that the diffraction peaks of VO_2F lose intensity, while new ones start growing at the same time. This can be especially well observed for the most intense reflection 012 of the rhombohedral phase (Figure S7†), where a shoulder appears and progressively grows at lower diffraction angle. Preliminary indexing of the

Accepted version:
Published in : " I*norganic Chemistry* **2020,** *59* (14), 10048-10058"
https://doi.org/10.1021/acs.inorgchem.0c01197

new reflections was successful with a rhombohedral structure having different cell parameters from these of pristine VO_2F. We believe that this Li_xVO_2F ($x > 0.9$) rhombohedral phase is an intermediate stage during the irreversible phase transformation after electrochemical lithiation of rhombohedral VO_2F (S.G. R-3c) to the cubic disordered rock-salt Li_2VO_2F (S.G. Fm-3m), which has been described by other authors.[11-13] Focusing on the solid-solution compositional range ($0 \leq x \leq 0.9$ in Li_xVO_2F), where structural changes are reversible, a sequential Rietveld refinement procedure was undertaken (Figures 6 and 7). All reflections have been indexed using the R-3c space group. Considering the results from *ex situ* neutron diffraction in the previous section, we undertook additional Rietveld refinements in the R3c space group. As above, refinements in this space did not produce improvement of the structural model, yielding the same lattice and crystal structure parameter.

The evolution of *a* and *c* lattice parameters and the cell volume are portrayed in Figure 6. Refined lattice parameters are a = 5.1302(1) Å and c = 13.0906(4) Å for x=0; a = 5.13060(2) Å and c = 13.120(1) Å for x=0.9. Overall, from VO_2F to $Li_{0.9}VO_2F$, the unit cell volume increases from V = 298.37(1) Å^3 to 299.10(3) Å^3. Interestingly, all these changes within the solid solution domain (Figure 6) are extremely small with little variation of the unit cell volume $\Delta V/V$ = +0.2%, which was subtly anisotropic ($\Delta a/a$ = -0.04%, $\Delta c/c$ = +0.22%). The small change in volume would contribute to the excellent cyclability detected in the solid solution domain reported in this work.

Accepted version:
Published in : " Inorganic Chemistry **2020,** *59* (14), 10048-10058"
https://doi.org/10.1021/acs.inorgchem.0c01197

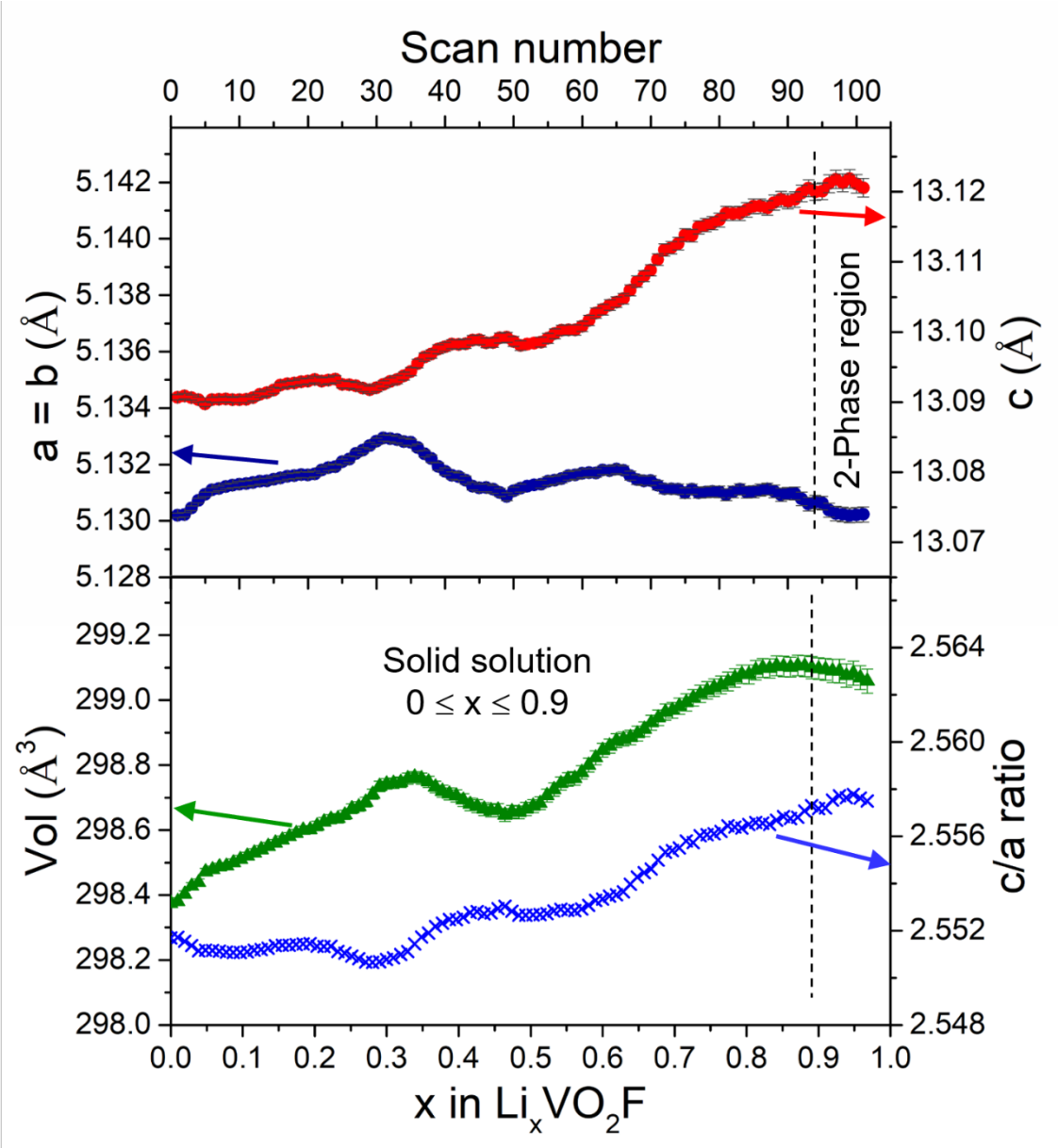

Figure 6: Parameters obtained from Rietveld refinement during reversible Li^+ intercalation in rhombohedral VO_2F in space group R-3c (reaction from pristine VO_2F to $Li_{0.9}VO_2F$). Unit cell parameters, unit cell volume and c/a ratio are shown.

The continuous changes for refined O/F anion x fractional atomic coordinate, V-O/F bond lengths and octahedral tilting angle V-O/F-V (Figure 7) were consistent with our neutron diffraction results. Note that the high quality of diffraction data made it possible to detect even rather subtle variations in structural parameters. These refinements show that the observed increase of the cell parameter *c* (Figure 6) upon Li insertion (between VO_2F and

Accepted version:
Published in : " I*norganic Chemistry* **2020,** *59* (14), 10048-10058"
https://doi.org/10.1021/acs.inorgchem.0c01197

$Li_{0.9}VO_2F$) is related with the increase of the mean V−O/F bond lengths from 1.888 Å in VO_2F to 1.904 Å in $Li_{0.9}VO_2F$ (Figure 7) along the V-Li-vacancy-V-Li-vacancy stacks of the face-shared M-O/F_6 bioctahedra. As mentioned above, the bond lengthening occurs in accordance with the progressive reduction of vanadium upon Li insertion. The combined effect of lengthening of V-O/F bonds, increasing octahedral twisting (measured by the anion x parameter, Figure 7) and increasing octahedral tilting (measured by decreasing V-O/F-V angle, Figure 7) explains the observed anisotropy of lattice parameters variations. The V-O/F-V angles, ideally 180º in the non-tilted ReO_3 structure, decreases continuously from 153.7º in VO_2F to 150.1º in $Li_{0.9}VO_2F$.

Accepted version:
Published in : " I*norganic Chemistry* **2020,** *59* (14), 10048-10058"
https://doi.org/10.1021/acs.inorgchem.0c01197

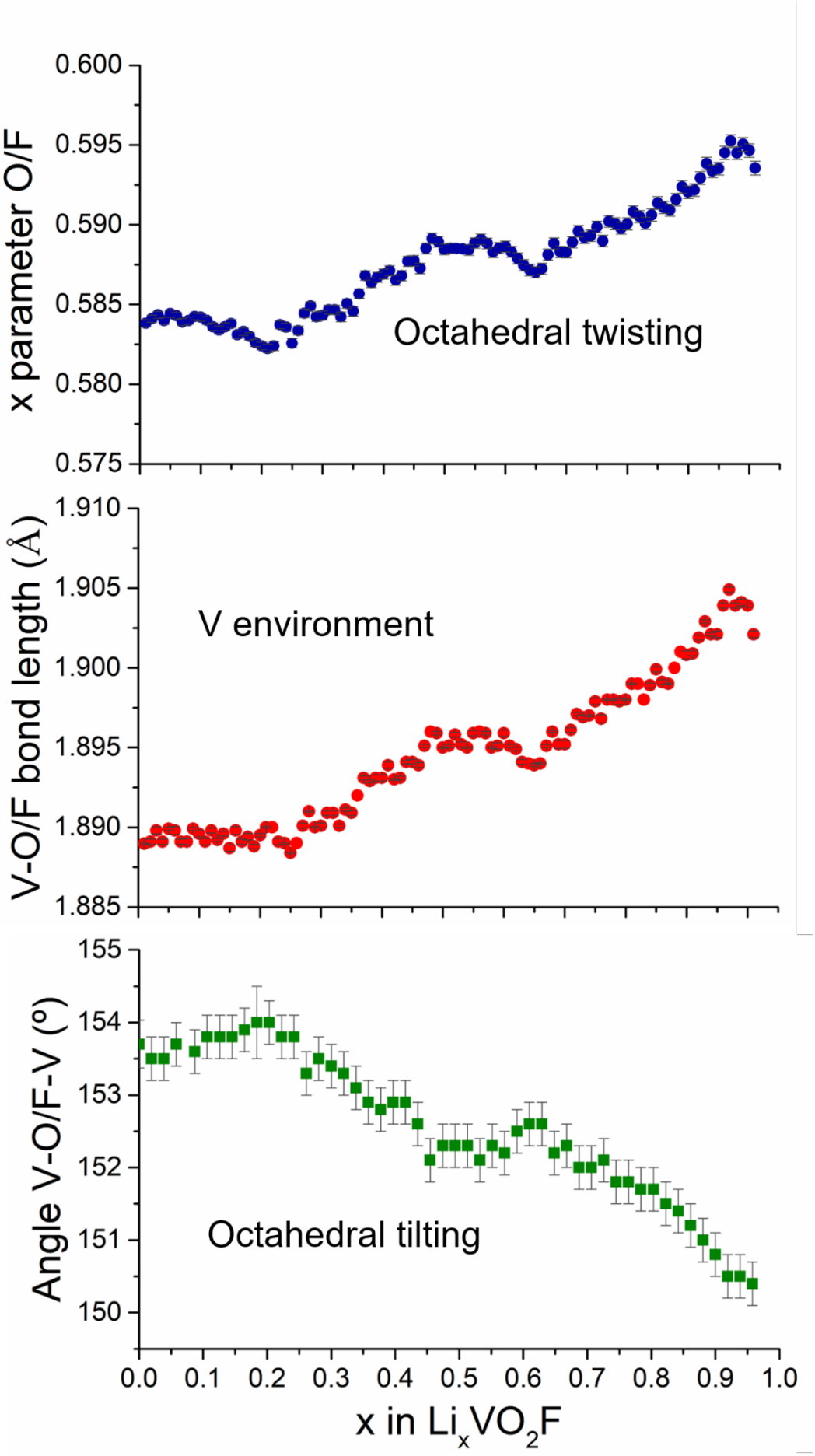

Accepted version:
Published in : " Inorganic Chemistry **2020,** *59* (14), 10048-10058"
https://doi.org/10.1021/acs.inorgchem.0c01197

Figure 7: Parameters obtained from Rietveld refinement (S.G. R-3c) during the solid solution reaction in Li_xVO_2F ($0 \leq x \leq 0.9$). Fractional atomic x coordinate of the anion O/F (top). Vanadium-anion O/F bond lengths obtained from refined anion atomic coordinates (bottom).

XAS

To unveil more details of lithium intercalation in this oxyfluoride and the role of fluorine, several Li_xVO_2F compositions were investigated by X-ray absorption spectroscopy. Figure 8 shows the composition of the samples selected for the XAS investigation. Besides the pristine sample (x=0), another two samples, obtained by potentiostatic discharge to 3.2 V ($Li_{0.39}VO_2F$) and 2.2 V ($Li_{0.9}VO_2F$) were investigated. Finally, a sample obtained after discharge to 2.2 V followed by full charge was also chosen. The composition of the fully charged material was estimated to be $Li_{0.1}VO_2F$ by coulometry, since a small coulombic inefficiency was observed upon charge.

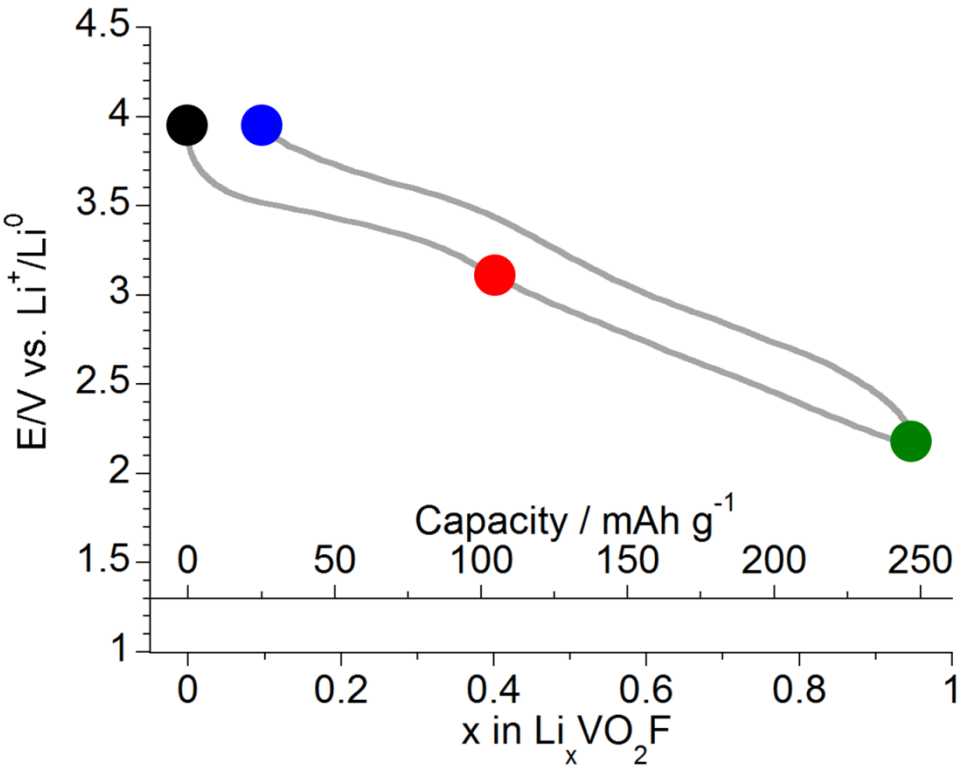

Accepted version:
Published in : " Inorganic Chemistry **2020,** *59* (14), 10048-10058"
https://doi.org/10.1021/acs.inorgchem.0c01197

Figure 8: The different *ex situ* samples synthesized for the XAS measurements are indicated on the voltage profile. Graphs presented in the XAS study will use the same color code.

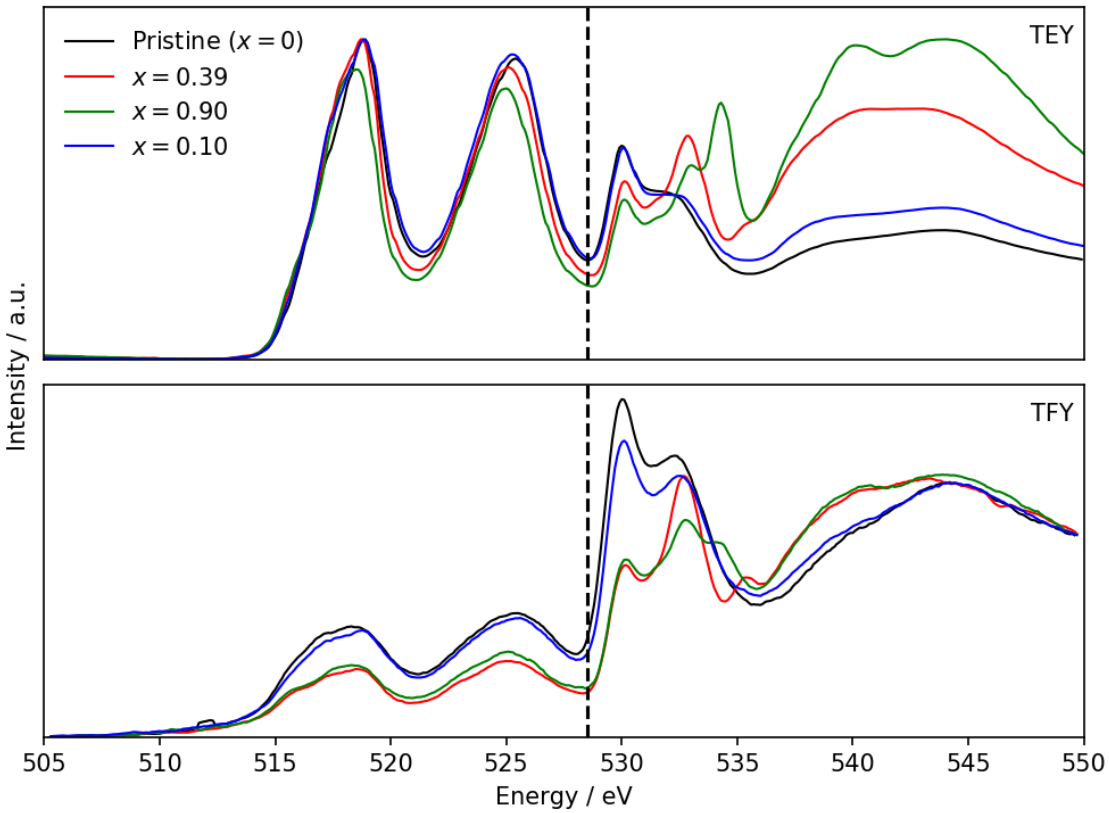

Figure 9: Vanadium *L*-edge and oxygen *K*-edge electron (top) and fluorescence yield (bottom) XAS signals of cycled Li_xVO_2F. The dotted line depicts the separation of the vanadium *L*-edge (left) and oxygen *K*-edge (right).

Figure 9 shows the V $L_{2,3}$- (505-529 eV) and oxygen *K*- edges (529 to 550 eV) of the different Li_xVO_2F. Furthermore, the regions between 515 to 521 eV and 521 to 528 eV correspond to V L_3 and L_2 edges, respectively, which correspond to multiplet transitions between V 2p and V 3d transitions that are dipole-allowed. The top spectra correspond to total electron yield detection (TEY) which is sensitive to the surface of the material

Accepted version:
Published in : " I*norganic Chemistry* **2020,** *59* (14), 10048-10058"
https://doi.org/10.1021/acs.inorgchem.0c01197

whereas the bottom spectra correspond to total fluorescence yield detection (TFY), sensitive to ~100 nm into the interior of the electrode and, therefore, more representative of the bulk. The relative intensities measured by TFY are distorted by self-absorption of fluorescent photons by the sample, but the qualitative trends are valid. From x=0 to x=0.9 (first discharge), the peaks of both V edges shifted to lower energy in both TEY and TFY spectra, indicating that vanadium is being reduced because the energy of the electron transition decreases with formal oxidation state. Upon deintercalation from x=0.9 to 0.1, the reversibility of the process, re-oxidation of V, is evidenced by the shifting of L_2 and L_3 peaks back to their original positions. Similar shifts and spectral shapes were found when comparing our measurements to reference data for V_2O_5 and VO_2 [37], confirming the formal change from V(V) to V(IV).

The spectral region from 536 eV to 550 eV in the O K-edge arises from unoccupied states due to the mixing of O 2*p* and V 4*sp* bands, and from the photoionization threshold. The spectra also display a pre-edge at lower energy, with peaks at 530.1 eV and 532.9 eV in pristine VO_2F. They can be assigned to the empty t_{2g} and e_g states arising for crystal field splitting of hybridized O 2p-V 3d states due to the octahedral coordination of vanadium by oxygen ligands.[37] The appearance of these two peaks is related to the existence of strong V-O covalent interactions.

The t_{2g} peak has a higher intensity than e_g, consistent with the expected multiplicity of the bands in d^0 state. Intercalation of lithium produces a switch in their relative intensities as evidenced in the spectrum of x=0.39 which is kept for higher degree of intercalation (x=0.9). This change is indicative of a decrease in the unoccupied t_{2g} states as a result of lithiation, confirming that O participates in the charge compensation mechanism through its covalent bond with V.

Accepted version:
Published in : " I*norganic Chemistry* **2020,** *59* (14), 10048-10058"
https://doi.org/10.1021/acs.inorgchem.0c01197

Aside from the changes in ratio of peak intensity at the pre-edge, a third peak appears at 534 eV in the spectrum at the highest level of lithiation. The significant distortion of the V-O/F_6 octahedra observed from analysis of diffraction data could lift the t_{2g}/e_g degeneracy, which would result in new pre-edge peaks as new non-degenerate O 2p-V 3d bands are created. However, an alternative hypothesis is that this peak arises from the formation of Li_2CO_3, which presents a pre-edge peak at similar energy.[38] While the overall changes are similar in TEY and TFY spectra, indicating consistency between surface and regions below it, the intensity of this pre-edge peak was much higher in the former than the latter. With the available evidence, it cannot be discarded that carbonate species were formed at the surface of the electrode during lithiation. Lastly, in parallel the overall relative intensity of the O pre-edge was found to decrease significantly compared to the post-edge, O 2p-V 4*sp* hybridized region (536 eV to 550 eV). This effect is consistent with the reduction of the compound, as injection of electrons would decrease the number of unoccupied O 2p-V 3d states, which act as centers for charge compensation. Indeed, a prior study of the O K-edge of several vanadium oxides showed that the relative intensity of the pre-edge decreases as the valence of vanadium decreases.[37] All the changes discussed reverse upon oxidation. However, the spectrum of the cycled sample is not a perfect match to the pristine state, consistent with the observation that full deintercalation was not reached under experimental conditions and the oxyfluoride retained a small amount of lithium (x=0.1).

Fig. 10 shows the F K-edge XAS spectra for all samples. The TEY spectra are also compared to LiF to be taken as a reference.

Similar to O, the spectra are split into two regions: the main absorption edge was tentatively assigned to the signals ranging from 688 eV and 705 eV, with a pre-edge located between 683 eV and 688 eV, based on previous analysis of transition metal

Accepted version:
Published in : " I*norganic Chemistry* **2020,** *59* (14), 10048-10058"
https://doi.org/10.1021/acs.inorgchem.0c01197

fluorides.[39] The latter arises from transitions to F 2p-V 3d hybridized orbitals while the former is assigned to hybridized F 2p-V4sp states, and the photoionization threshold. A first interesting finding is the mere existence of the pre-edge. It strongly suggests the existence of covalent interactions between V and F in Li_xVO_2F, as observed in transition metal fluorides at lower formal oxidation states.[16,39] For comparison the XAS spectrum of the highly ionic LiF does not show any pre-edge. No signals were observed at these energies for the fluorinated binder used in the electrodes, either (Figure S8†). The spectrum of this binder caused some interference above the absorption edge in the TEY spectra, suggesting that the surface of the electrodes was rich in it, but the TFY spectra were clearly different, validating the following analysis.

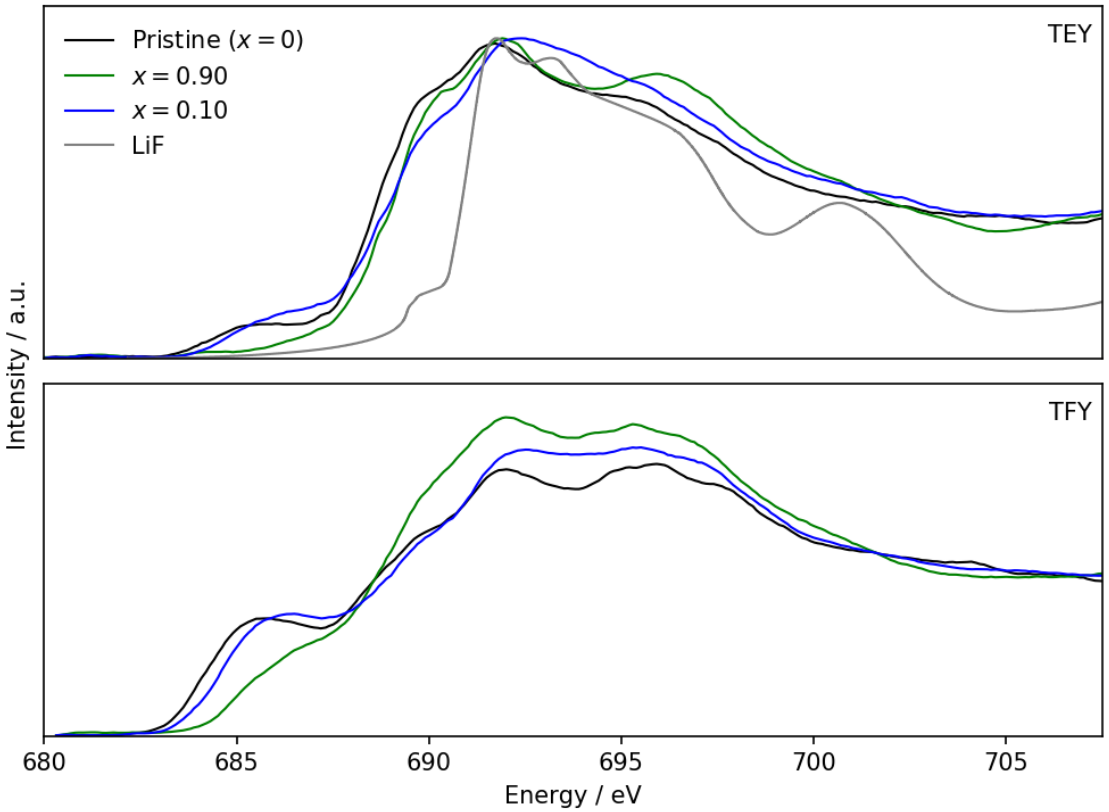

Accepted version:
Published in : " I*norganic Chemistry* **2020,** *59* (14), 10048-10058"
https://doi.org/10.1021/acs.inorgchem.0c01197

Figure 10: Fluorine *K*-edge electron (top) and fluorescence (bottom) XAS signals of cycled Li_xVO_2F.

The most visible effect of lithium insertion on the F K-edge spectra is the significant decrease in intensity of the pre-edge signal, both in TFY and TEY modes. The decrease reflects the reduction of the compound, which creates new occupied states with a F 2p-V 3d character, which are no longer available for electronic transitions during the XAS measurement. A second factor that can contribute to this change is the decrease in the degree of covalency of the V-F bond, so that the states involved in charge compensation have a stronger V character than F compared to the pristine compound. No evidence of the appearance of signals related to the formation of LiF were observed even in the TEY spectra, indicating that lithiation proceeds through an intercalation mechanism, not conversion. The similarity in the trends in TEY and TFY indicates that there was minimal, if any, interfacial reactivity to form fluorinated species. In the TFY spectrum, which is clearly free from interference, the decrease is accompanied by a shift to higher energy of the pre-edge transition, and an increase in intensity at 690 eV. The two extended features centered at ca. 692 and 696 eV did not seem to substantially move. Therefore, it is not clear if the ionization threshold was affected by reduction. The changes are reversed after re-oxidation, but not completely back to the pristine state, again consistent with the slight coulombic inefficiency observed in the electrochemical data.

Figure S8† shows the Kynarflex F K-edge plotted with pristine VO_2F. The difference of pre-edge peak in both the TEY and TFY spectrum shows covalency of VO_2F is not present in the Kynarflex binder. Carbon black had no visible contribution in the O K-edge region.

Accepted version:
Published in : " I*norganic Chemistry* **2020,** *59* (14), 10048-10058"
https://doi.org/10.1021/acs.inorgchem.0c01197

Conclusions

In this work, high resolution neutron diffraction together with high angular and intensity resolution synchrotron radiation diffraction, realized *operando* on Li batteries, was used to study in detail the structural evolution of VO_2F upon insertion of one Li^+ in the high voltage range, 3.9 - 2.2 V. Both pristine VO_2F and lithiathed Li_xVO_2F ($0 < x \leq 1$) compounds have similar lattice parameters, with lithium intercalation only producing a slight increase of c/a ratio and very little change in cell volume. These observations explain the excellent cyclability of the compound when cycled in the solid solution region. However, a closer examination reveals a continuous transition of the originally cubic-like close packing of anions found in VO_2F, space group R-3c, towards hexagonal close packing in $LiVO_2F$ with space group R3c to accommodate the preferred crystal chemistry of the alkali metal in the structure.

We have further evaluated the redox changes of VO_2F upon Li uptake. Li insertion not only produces reduction of V(V) but is accompanied by a change of covalent interactions with both O^{2-} and F^- anions as deduced from X-ray absorption spectroscopy. By comparing changes in electronic states of all the elements in the compound, it clarifies the critical role of both anions, O and F, in the charge compensation, through their covalent interactions with the 3d states of V. The clear evidence of participation of F challenges existing assumptions that its high electronegativity renders this anion largely a spectator in the redox reaction.

Accepted version:
Published in : " I*norganic Chemistry* **2020,** *59* (14), 10048-10058"
https://doi.org/10.1021/acs.inorgchem.0c01197

The 2p states of both O and F mix with V 3d states. The degree of mixing is highest for the pristine compound, which means that injection of electrons during intercalation involves both metal and ligands. The degree of mixing seemed to decrease upon reduction of the compound. The comparison of V^{V}/V^{IV} vs Li^{I}/Li reduction potential in VO_2F with respect to V_2O_5 indicates that the use of the *rule of thumb* to greatly increase reduction potential by introducing highly electronegative ligands is overly simplistic, and that both the particulars of the covalent interactions in the compound and the energetics of the sites available for intercalation must be considered. This work expands our understanding of intercalation chemistry to mixed anion compounds, a family that is the object of increase scrutiny in the quest for novel cathodes for Li-ion batteries with high energy density.

Author Information

Corresponding Authors

akuhn@ceu.es

Conflicts of interest

There are no conflicts of interest to declare.

Acknowledgements

José Manuel Gallardo-Amores (high-pressure laboratory UCM) is acknowledged for synthesis of the VO_2F samples. The staff of the mechanic workshop of Universidad Complutense Madrid is also acknowledged for manufacturing components of the *in situ* cell. We thank Agencia Estatal de Investigación (AEI)/Fondo Europeo de Desarrollo Regional (FEDER/UE) for funding the project MAT2016-78632-C4-1-R. The synchrotron diffraction experiments at ALBA were funded through the proposal with

Accepted version:
Published in : " I*norganic Chemistry* **2020,** *59* (14), 10048-10058"
https://doi.org/10.1021/acs.inorgchem.0c01197

reference number 2016091904. This research used resources of the Advanced Photon Source, a U.S. Department of Energy (DOE) Office of Science User Facility operated for the DOE Office of Science by Argonne National Laboratory under Contract No. DE-AC02-06CH11357.

References

(1) Deng, D. Li-ion batteries: basics, progress, and challenges. *Energy Sci. Eng.*, **2015**, *3* (5), 385-418.

(2) Tarascon, J. M.; Armand M. Issues and challenges facing rechargeable lithium batteries. *Nature*, **2001**, *414*, 359-367.

(3) Radin, M. D.; Hy, S.; Sina, M.; Fang, C.; Liu, H.; Vinckeviciute, J.; Zhang, M.; Whittingham, M. S.; Meng, Y. S.; Van der Ven, A. Narrowing the Gap between Theoretical and Practical Capacities in Li-Ion Layered Oxide Cathode Materials. *Adv. Energy Mater.*, **2017**, *7* (20), 1602888.

(4) Goodenough, J. B.; Park, K. S. The Li-ion rechargeable battery: a perspective. *J. Am. Chem. Soc.*, **2013**, *135* (4), 1167-1176.

(5) Yi, T.-F.; Yanga, S.-Y.; Xie, Y. Recent advances of $Li_4Ti_5O_{12}$ as a promising next generation anode material for high power lithium-ion batteries. *J. Mater. Chem. A*, **2015**, *3*, 5750-5777.

(6) Zhu, G.-N.; Wang, Y.-G.; Xia, Y.-Y. Ti-based compounds as anode materials for Li-ion batteries. *Energy Environ. Sci.*, **2012**, *5*, 6652-6667.

(7) Gocheva, I. D.; Doi, T.; Okada S.; Yamaki, J. I. Electrochemical properties of trirutile-type Li_2TiF_6 as cathode active material in Li-ion batteries. *Electrochemistry*, **2010**, *78* (5), 471-474.

Accepted version:
Published in : " I*norganic Chemistry* **2020,** *59* (14), 10048-10058"
https://doi.org/10.1021/acs.inorgchem.0c01197

(8) Basa, A.; Gonzalo, E. G.; Kuhn, A.; García-Alvarado, F. Facile synthesis of β-Li_3VF_6: A new electrochemically active lithium insertion material. *J. Power Sources*, **2012**, *207*, 160-165.

(9) Deng, D. Transition Metal Oxyfluorides for Next-Generation Rechargeable Batteries. *ChemNanoMat*, **2017**, *3* (3), 146-159.

(10) Pérez-Flores, J. C.; Villamor, R.; Avila-Brande, D.; Gallardo Amores, J. M.; Morán, E.; Kuhn, A.; García-Alvarado, F. VO_2F: a new transition metal oxyfluoride with high specific capacity for Li ion batteries. *J. Mater. Chem. A*, **2015**, *3*, 20508-20515.

(11) Cambaz, M. A.; Vinayan, B. P.; Clemens, O.; Munnangi, A. R.; Chakravadhanula, V. S. K.; Kubel, C.; Fichtner, M. Vanadium Oxyfluoride/Few-Layer Graphene Composite as a High-Performance Cathode Material for Lithium Batteries. *Inorg. Chem.*, **2016**, *55* (8), 3789-3796.

(12) Chen, R.; Maawad, E.; Knapp, M.; Ren, S.; Beran, P.; Witter, R.; Hempelmann, R. Lithiation-driven structural transition of VO_2F into disordered rock-salt Li_xVO_2F. *RSC Adv.*, **2016**, *6*, 65112-65118.

(13) Chen, R.; Ren, S.; Knapp, M.; D. Wang, D.; Witter, R.; Fichtner, M.; Hahn, H. Disordered Lithium-Rich Oxyfluoride as Stable Host for Enhanced Li+ Intercalation Storage. *Adv. Energy Mater.*, **2015**, *5* (9), 1401814.

(14) Cambaz, M. A.; Vinayan, B. P.; Pervez, S. A.; Johnsen, R. E.; Geßwein, H.; Guda, A. A.; Rusalev, Y. V.; Kinyanjui, M. K.; Kaiser, U.; Fichtner, M. Suppressing Dissolution of Vanadium from Cation-Disordered $Li_{2-x}VO_2F$ via a Concentrated Electrolyte Approach. *Chem. Mater.*, **2019**, *31* (19), 7941-7950.

(15) Wang, X.; Lin, Y.-C.; Zhou, H.; Omenya, F.; Chu, I.-H.; Karki, K.; Sallis, S.; Rana, J.; Piper, L. F. J.; Chernova, N. A.; Ong, S. P.; Whittingham, M. S. Structural

Accepted version:
Published in : " I*norganic Chemistry* **2020,** *59* (14), 10048-10058"
https://doi.org/10.1021/acs.inorgchem.0c01197

Changes in a High-Energy Density VO_2F Cathode upon Heating and Li Cycling. *ACS Appl. Energy Mater.*, **2018**, *1* (9), 4514-4521.

(16) Olalde-Velasco, P.; Jiménez-Mier, J.; Denlinger, J. D.; Hussain, Z.; Yang, W. L. Direct probe of Mott-Hubbard to charge-transfer insulator transition and electronic structure evolution in transition-metal systems. *Phys. Rev. B*, **2011**, *83*, 241102(R).

(17) Yang, W.; Liu, X.; Qiao, R.; Olalde-Velasco, P.; Spear, J. D.; Roseguo, L.; Pepper, J. X.; Chuang, Y.-D.; Denlinger, J. D.; Hussain, Z. Key electronic states in lithium battery materials probed by soft X-ray spectroscopy. *J. Electron Spect. Rel. Phen.*, **2013**, *190* (A), 64-74.

(18) Li, L.; Castro, F. C.; Park, J. S.; Li, H.; Lee, E.; Boyko, T. D.; Freeland, J. W.; Yao, Z.; Fister, T. T.; Vinson, J.; Shirley, E. L.; Wolverton, C.; Cabana, J.; Dravid, V. P.; Thackeray, M. M.; Chan, M. K. Y. Probing Electrochemically Induced Structural Evolution and Oxygen Redox Reactions in Layered Lithium Iridate. *Chem. Mater.*, **2019**, *31* (12), 4341-4352.

(19) Filonenko, V. P.; Sundberg, M.; Werner, P.-E.; Zibrov, I. P. Structure of a high-pressure phase of vanadium pentoxide, β-V_2O_5. *Acta Cryst. B*, **2004**, *60* (4), 375-381.

(20) Hoelzel, M.; Senyshyn, A; Juenke, N.; Boysen, H.; Schmahl, W.; Fuess, H. High-resolution neutron powder diffractometer SPODI at research reactor FRM II. *Nucl. Instr.*, **2012**, *A 667* (1), 32-37.

(21) Rietveld, H. The crystal structure of some alkaline earth metal uranates of the type M_3UO_6. *Acta Crystallogr.*, **1966**, *20* (4), 508-513.

(22) Rietveld, H. Line profiles of neutron powder-diffraction peaks for structure refinement. *Acta Crystallogr.*, **1967**, *22* (1), 151-152.

Accepted version:
Published in : " I*norganic Chemistry* **2020,** *59* (14), 10048-10058"
https://doi.org/10.1021/acs.inorgchem.0c01197

(23) Rodriguez-Carvajal, J. Recent advances in magnetic-structure determination by neutron powder diffraction. *Physica B: Condensed Matter*, **1993**, *192* (1-2), 55-69.

(24) Sears, V. F. Neutron scattering lengths and cross sections. *Neutron News*, **1992**, *3* (3), 26-37.

(25) Momma K.; Izumi, F. VESTA 3 for three-dimensional visualization of crystal, volumetric and morphology data. *J. Appl. Cryst.*, **2011**, *44* (6), 1272-1276.

(26) Kuhn, A.; Pérez-Flores, J. C.; Hoelzel, M.; Baehtz, C.; Sobrados, I.; Sanz, J.; García-Alvarado, F. Comprehensive investigation of the lithium insertion mechanism of Na2Ti6O13 anode material for Li-ion batteries. *J. Mater. Chem. A*, **2018**, *6*, 443-455.

(27) Pérez-Flores, J. C.; Baehtz, C.; Kuhn, A.; Garcia-Alvarado, F. Hollandite-type TiO2: a new negative electrode material for sodium-ion batteries. *J. Mater. Chem. A*, **2014**, 2, 1825-1833.

(28) Bianchini, M.; Fauth, F.; Brisset, N.; Weill, F.; Suard, E.; Masquelier, C.; Croguennec, L. Comprehensive Investigation of the $Na_3V_2(PO_4)_2F_3$–$NaV_2(PO_4)_2F_3$ System by Operando High Resolution Synchrotron X-ray Diffraction. *Chem. Mater.*, **2015**, *27* (8), 3009-3020.

(29) Cullity, B. D.; Stock, S.R. *Elements of X-ray Diffraction*. Vol. 3 (Prentice Hall Upper Saddle River, NJ, 2001).

(30) Siegel, S. The structure of TiF_3. *Acta Crystallogr.*, **1956**, *9*, 684.

(31) Jack, K. H.; Gutmann, V. The crystal structure of vanadium trifluoride VF_3. *Acta Crystallogr.*, **1951**, *4*, 246-249.

(32) Knox, K. Structures of chromium(III) fluoride. *Acta Crystallogr.*, **1960**, *13*, 507-508.

Accepted version:
Published in : " I*norganic Chemistry* **2020,** *59* (14), 10048-10058"
https://doi.org/10.1021/acs.inorgchem.0c01197

(33) Hepworth, M. A.; Jack, K.H.; Peacock, R.D.; Westland, G. J. The crystal structures of the trifluorides of iron, cobalt, ruthenium, rhodium, palladium and iridium. *Acta Crystallogr.*, **1957**, *10*, 63-69.

(34) Cava, R. J. Structural aspects of lithium insertion in oxides: Li_xReO_3 and $Li_2FeV_3O_8$. *Solid State Ionics*, **1981**, *5*, 323-326.

(35) Abrahams, S. C.; Reddy, J. M.; Bernstein, J. L. Ferroelectric lithium niobate. 3. Single crystal X-ray diffraction study at 24°C. *J. Phys. Chem. Solids*, **1966**, *27* (6-7), 997-1012.

(36) Cava, R. J.; Santoro, A.; Murphy, D. W.; Zahurak, S. M.; Roth, R. S. The structures of lithium-inserted metal oxides: $LiReO_3$ and Li_2ReO_3. *J. Solid State Chem.*, **1982**, *42* (3), 251-262.

(37) Abbate, M.; Pen, H.; Czyżyk, M. T.; de Groot, F. M. F.; Fuggle, J. C.; Ma, Y. J.; Chen, C. T.; Sette, F.; Fujimori, A.; Ueda, Y.; Kosuge, K. Soft X-ray absorption spectroscopy of vanadium oxides. *J. Electron Spect. Rel. Phen.*, **1993**, *62* (1-2), 185-195.

(38) Qiao, R.; Chuang, Y.-D.; Yan, S. W. Soft X-Ray Irradiation Effects of Li_2O_2, Li_2CO_3 and Li_2O Revealed by Absorption Spectroscopy. *PLoS ONE*, **2012**, *7*(11): e49182. https://doi.org/10.1371/journal.pone.0049182.

(39) Olalde-Velasco, P., Jiménez-Mier, J.; Denlinger, J.; Yang, W.-L. Atomic multiplets at the L2,3 edge of 3d transition metals and the ligand K edge in x-ray absorption spectroscopy of ionic systems. *Phys. Rev. B*, **2013**, *87* (24), 245136.

Accepted version:
Published in : " Inorganic Chemistry **2020,** *59* (14), 10048-10058"
https://doi.org/10.1021/acs.inorgchem.0c01197

For Table of Contents Only

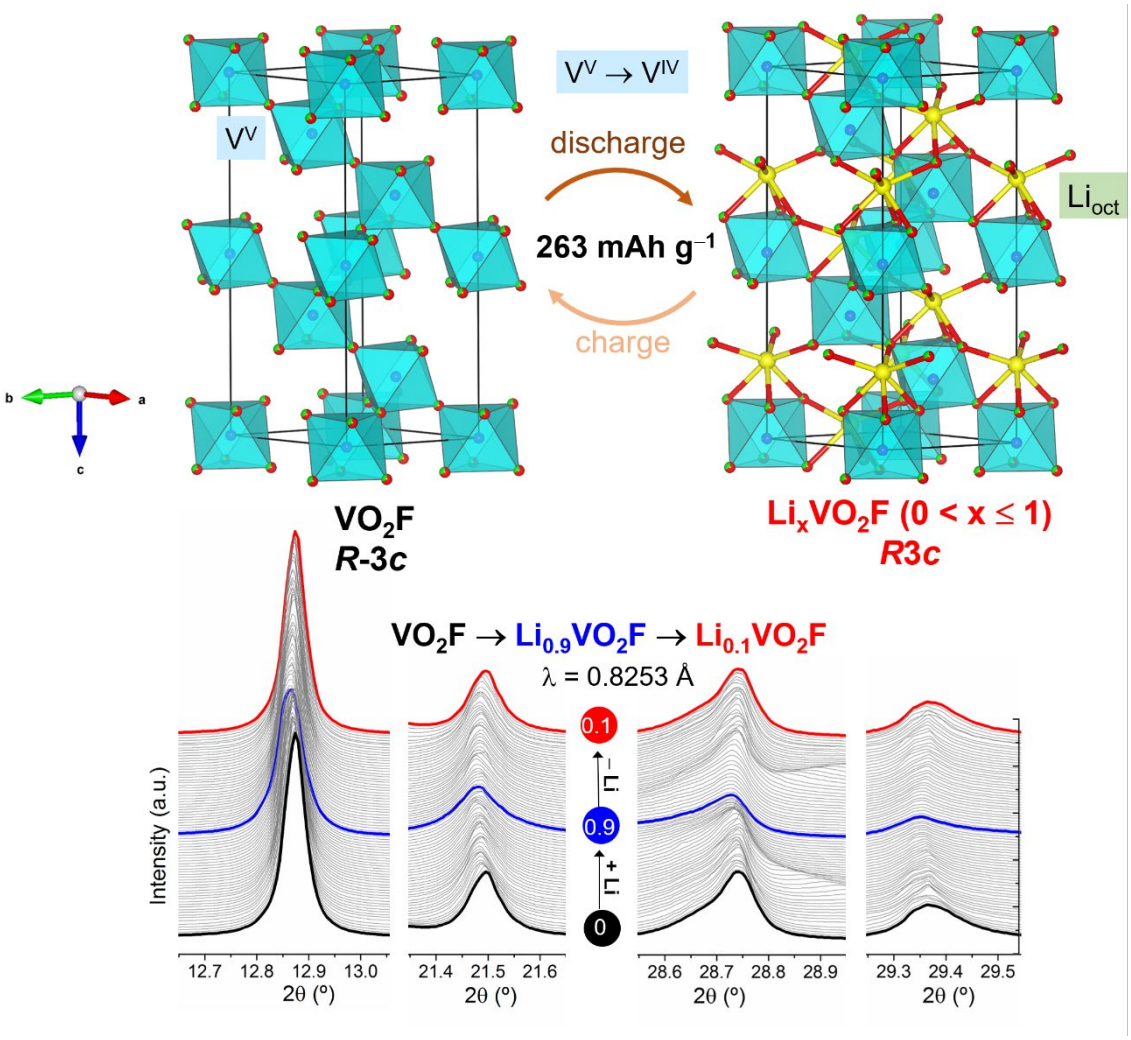

The exact Li^+ insertion mechanism in rhombohedral VO_2F is unraveled using a combination of *ex situ* neutron diffraction and high angular synchrotron diffraction measurements performed *operando* on a lithium battery. The clear evidence of participation of F from XAS challenges existing assumptions that its high electronegativity renders this anion largely a spectator in the redox reaction.